



Room-temperature waveguide integrated quantum register in a semiconductor photonic platform

Received: 11 September 2024

Accepted: 13 November 2024

Published online: 26 November 2024

Check for updates

Haibo Hu^{1,2,10}, Yu Zhou^{1,3,10}✉, Ailun Yi^{1,4,5,10}, Tongyuan Bao¹, Chengying Liu¹, Qi Luo¹, Yao Zhang¹, Zi Wang¹, Qiang Li^{6,7}, Dawei Lu^{1,3,8}, Zhengtong Liu^{1,2}, Shumin Xiao^{1,2,3,9}, Xin Ou^{1,4,5}✉ & Qinghai Song^{1,2,3,9}✉

Quantum photonic integrated circuits are reshaping quantum networks and sensing by providing compact, efficient platforms for practical quantum applications. Despite continuous breakthroughs, integrating entangled registers into photonic devices on a CMOS-compatible platform presents significant challenges. Herein, we present single electron-nuclear spin entanglement and its integration into a silicon-carbide-on-insulator (SiCOI) waveguide. We demonstrate the successful generation of single divacancy electron spins and near-unity spin initialization of single ¹³C nuclear spins. Both single nuclear and electron spin can be coherently controlled and a maximally entangled state with a fidelity of 0.89 has been prepared under ambient conditions. Based on the nanoscale positioning techniques, the entangled quantum register has been further integrated into SiC photonic waveguides for the first time. We find that the intrinsic optical and spin characteristics of the register are well preserved and the fidelity of the entangled state remains as high as 0.88. Our findings highlight the promising prospects of the SiCOI platform as a compelling candidate for future scalable quantum photonic applications.

Nuclear-electron quantum registers are essential components of multi-node quantum networks^{1,2} and quantum sensing^{3–5}. These registers, with electron-coupled nuclear spins serving as memory qubits or sensors, play a crucial role in network operations^{1,2,5}. Color centers in diamonds have been at the forefront of constructing quantum networks, with significant advancements and achievements realized over

the past decades with two main approaches^{1,2,6–10}. The first approach entails the entanglement of nitrogen-vacancy centers in bulk diamonds at distant sites using herald protocols^{1,6–8}. A more integrated strategy incorporates silicon vacancy⁹ and proximal nuclear spins² within diamond nanophotonics, marking significant steps in quantum network construction. At the same time, quantum sensing using

¹Ministry of Industry and Information Technology Key Lab of Micro-Nano Optoelectronic Information System, Guangdong Provincial Key Laboratory of Semiconductor Optoelectronic Materials and Intelligent Photonic Systems, Harbin Institute of Technology, Shenzhen, China. ²Pengcheng Laboratory, Shenzhen, China. ³Quantum Science Center of Guangdong-HongKong-Macao Greater Bay Area (Guangdong), Shenzhen, China. ⁴State Key Laboratory of Materials for Integrated Circuits, Shanghai Institute of Microsystem and Information Technology, Chinese Academy of Sciences, Shanghai, China. ⁵The Center of Materials Science and Optoelectronics Engineering, University of Chinese Academy of Sciences, Beijing, China. ⁶Institute of Advanced Semiconductors, Zhejiang Provincial Key Laboratory of Power Semiconductor Materials and Devices, ZJU-Hangzhou Global Scientific and Technological Innovation Center, Hangzhou, Zhejiang, China. ⁷State Key Laboratory of Silicon Materials and Advanced Semiconductors & School of Materials Science and Engineering, Zhejiang University, Hangzhou, China. ⁸Shenzhen Institute for Quantum Science and Engineering and Department of Physics, Southern University of Science and Technology, Shenzhen, China. ⁹Collaborative Innovation Center of Extreme Optics, Shanxi University, Taiyuan, Shanxi, China. ¹⁰These authors contributed equally: Haibo Hu, Yu Zhou, Ailun Yi. ✉e-mail: zhousy2022@hit.edu.cn; ouxin@mail.sim.ac.cn; qinghai.song@hit.edu.cn

ARTICLE



<https://doi.org/10.1038/s41467-021-26205-y>

OPEN

Rapid and unconditional parametric reset protocol for tunable superconducting qubits

Yu Zhou^{1,4}, Zhenxing Zhang^{1,4}, Zelong Yin¹, Sainan Huai¹, Xiu Gu¹, Xiong Xu¹, Jonathan Allcock¹, Fuming Liu¹, Guanglei Xi¹, Qiaonian Yu¹, Hualiang Zhang¹, Mengyu Zhang¹, Hekang Li^{1,2,3}, Xiaohui Song^{2,3}, Zhan Wang^{2,3}, Dongning Zheng^{2,3}, Shuoming An¹✉, Yarui Zheng¹ & Shengyu Zhang¹

Qubit initialization is a critical task in quantum computation and communication. Extensive efforts have been made to achieve this with high speed, efficiency and scalability. However, previous approaches have either been measurement-based and required fast feedback, suffered from crosstalk or required sophisticated calibration. Here, we report a fast and high-fidelity reset scheme, avoiding the issues above without any additional chip architecture. By modulating the flux through a transmon qubit, we realize a swap between the qubit and its readout resonator that suppresses the excited state population to $0.08\% \pm 0.08\%$ within 34 ns (284 ns if photon depletion of the resonator is required). Furthermore, our approach (i) can achieve effective second excited state depletion, (ii) has negligible effects on neighboring qubits, and (iii) offers a way to entangle the qubit with an itinerant single photon, useful in quantum communication applications.

¹Tencent Quantum Laboratory, Tencent, Shenzhen, Guangdong 518057, China. ²Beijing National Laboratory for Condensed Matter Physics, Institute of Physics, Chinese Academy of Sciences, Beijing 100190, China. ³School of Physical Sciences, University of Chinese Academy of Sciences, Beijing 100049, China. ⁴These authors contributed equally. Yu Zhou and Zhenxing Zhang ✉email: shuoming@tencent.com

Qubit initialization is fundamental and crucial for many quantum algorithms and quantum information processing tasks. The ability to quickly reset qubits to the zero state is one of DiVincenzo's essential criteria for building a quantum computer¹ and is critical for quantum error correction^{2–4}, where the reset of syndrome qubits needs to be accomplished with high fidelity in the time scale of a single qubit pulse. Furthermore, significant reduction of state preparation and measurement (SPAM) errors can be achieved by evacuating residual excited state populations with high fidelity^{5,6}. The simplest way to reset qubits is to passively wait for them to de-excite, but as qubit relaxation times increase beyond 100 μs^{7,8}, this method becomes impractically slow. Alternatively, active reset implementations can shorten the wait time between cycles and significantly improve computational efficiency^{9,10}.

Various reset protocols for superconducting qubits have been proposed which fall into two main types: measurement- and non-measurement-based protocols. In measurement-based schemes, a qubit is measured and either heralded in the ground state¹¹, or else is found to be in the excited state and reset via a conditional π-pulse^{6,12–15}. These protocols depend heavily on measurement fidelity and suffer from measurement-induced state mixing^{5,16}. In addition, the hardware implementation of necessary short-latency feedback loops is also a challenge. In non-measurement based protocols, qubits are coupled to a lossy environment, usually a resonator. While numerous approaches to this have been proposed, they each suffer from their own drawbacks. For instance, in one such approach, flux control^{17,18} is used to rapidly tune the qubit frequency to that of the resonator. However, this process significantly affects neighboring qubits via crosstalk^{19,20}. Another approach is based on a microwave-induced interaction between the qubit and a low-quality factor resonator^{9,21}. However, the involvement of the second excited state $|f\rangle$ makes these schemes complicated and necessitates sophisticated calibration. Furthermore, intense microwave driving is required to activate the required cavity-assisted Raman processes^{21–23}, affecting adjacent qubits as well. In²¹, an additional resonator is required to achieve the best performance. In contrast to the above methods, the driven reset scheme proposed in¹⁰ is free from flux control and complicated pulses. On the other hand, this protocol requires that the resonator dissipation rate κ_r be smaller than the dispersive shift χ , imposing a trade-off between readout speed and fidelity.

In this work, we demonstrate a rapid and unconditional parametric reset scheme for tunable superconducting qubits. By parametric modulation of the qubit frequency, a controllable interaction is generated between the qubit and a lossy readout resonator. This interaction unconditionally transfers the qubit excitation to the resonator and thus resets the qubit on demand. Using this method, we can suppress the residual excited population to $0.08\% \pm 0.08\%$ within 34 ns. We also demonstrate effective $|f\rangle$ state depletion in the case when leakage to higher states is non-negligible. Our protocol only involves AC modulation of at most two frequencies and does not need sophisticated calibration. Moreover, it has a negligible effect on subsequent gates and other qubits. It is compatible with circuit quantum electrodynamics systems^{24–26} and can be applied to all frequency-tunable superconducting qubits, requiring no additional hardware or modifications to chip components. The method also imposes no restriction on operation flux position or specific system parameters such as resonator dissipation rate κ_r or dispersive shift.

Results

Theory. Our qubit reset protocol is based on a parametric activated interaction between a tunable qubit and a rapidly decaying

resonator. Such a parametric modulation induces an effective tunable coupling between the qubit and other quantum systems such as another qubit or resonator^{27–29} and has been used to implement multi-qubit quantum gates^{30–35}, state transfer^{36,37}, switches for quantum circuits³⁸ and parity measurements³⁹. In our reset protocol, the parametric modulation induces Rabi oscillations between $|e, 0\rangle$ and $|g, 1\rangle$, where $|s, l\rangle$ denotes the tensor product of the qubit state $|s\rangle$ (the cases $|s\rangle = |g\rangle$ and $|s\rangle = |e\rangle$ correspond to the ground and excited states, respectively) and the resonator Fock state $|l\rangle$. When the qubit is excited, as illustrated in Fig. 1a, the population can be transferred from the qubit ($|e, 0\rangle$) to the resonator ($|g, 1\rangle$), which then rapidly decays to the target state $|g, 0\rangle$ at decay rate κ_r , which is mainly due to the large photon emission rate of the readout resonator.

We consider a qubit-resonator coupled system described by the Jaynes-Cummings model. In the dispersive regime, there is no population exchange due to the large detuning between the qubit and the resonator. The external flux Φ is modulated as $\Phi(t) = \bar{\Phi} + \Phi_m \cos(\omega_m t + \theta_m)$, where $\bar{\Phi}$ is the parking flux and $\Phi_m, \omega_m, \theta_m$ is the flux modulation amplitude, frequency and phase, respectively. Due to the nonlinear dependence of the qubit frequency on the flux bias, the qubit frequency $\omega_q(t)$ is, in general, described by a Fourier series with non-trivial higher-order terms, i.e. $\omega_q(t) = \bar{\omega}_q + \sum_{k=1} A_m^{(k)} \cos[k(\omega_m t + \theta_m)]$ where $A_m^{(k)}$ are the Fourier coefficients and $\bar{\omega}_q$ is the average frequency in the presence of the modulation³¹. In the case of small modulation, we take the leading term of the qubit frequency as an approximation, i.e. $\omega_q(t) \approx \bar{\omega}_q + A_m^{(1)} \cos[\alpha(\omega_m t + \theta_m)]$, where $\alpha = 1$ for the qubit parked away from the sweet spot, and $\alpha = 2$ for the qubit parked in the sweet spot (in the latter case the odd Fourier coefficients $A_m^{(2k+1)}$ vanish³¹). The oscillation of the qubit frequency induces a series of sidebands $\bar{\omega}_q + n\omega_m$, where n is an integer. When the frequency of one sideband satisfies the constraints $n\omega_m = -\bar{\Delta} = \omega_r - \bar{\omega}_q$, the transition between the states $|e, l\rangle$ and $|g, l+1\rangle$ is activated. The effective coupling strength can be derived as $g_n = \bar{g}_{qr} J_n(\frac{A_m^{(1)}}{\omega_m}) e^{i\beta_n}$, where \bar{g}_{qr} is the averaged coupling strength between the qubit and the resonator during the modulation, $J_n(x)$ are Bessel functions of the first kind, and $\beta_n = n\theta_m - \frac{A_m^{(1)}}{\alpha\omega_m} \sin(\alpha\theta_m)$ is the interaction phase³¹.

We consider the single excitation subspace spanned by $\{|e, 0\rangle, |g, 1\rangle\}$, within which the dynamics of the reset protocol can be modeled by the non-Hermitian Hamiltonian

$$H_{\text{eff}} = \begin{bmatrix} 0 & |g_n| e^{i\beta_n} \\ |g_n| e^{-i\beta_n} & -i\kappa_r/2 \end{bmatrix}, \quad (1)$$

where $|g_n|$ is the absolute value of g_n , and the non-Hermitian term $-i\kappa_r/2$ accounts for the decay of the photon in the resonator. The population evolution can be expressed as $P_{s|s_0}(t) = |\langle s|e^{-iH_{\text{eff}}t}|s_0\rangle|^2$, where the system is initially prepared in the state $|s_0\rangle$, and $|s\rangle$ is one of the states $\{|e, 0\rangle, |g, 1\rangle\}$.

The real parts of the eigenvalues $\{\lambda_k\}$ of H_{eff} determine the oscillation rate of $P_{s|s_0}(t)$, while the imaginary parts of $\{\lambda_k\}$ determine the exponential decay rates. We define the reset rate $\Gamma = 2\min_k(|\text{Im}[\lambda_k]|)$ as it is the smallest value of the decay rates and determines the overall protocol reset speed. Three different regimes are possible – corresponding to overdamped, critically damped and underdamped oscillations of $P_{s|s_0}(t)$, respectively – and our qubit reset works in all three regimes. For small modulation amplitudes, i.e., $|g_n| < \kappa_r/4$, the reset is in the overdamped regime where the excited state population decays without oscillating. In this

REVIEW ARTICLE | JULY 01 2025

Silicon carbide: A promising platform for scalable quantum networks

Special Collection: **Quantum Light**

Yu Zhou   ; Junhua Tan; HaiBo Hu  ; Sikai Hua  ; Chunhui Jiang  ; Bo Liang  ; Tongyuan Bao; Xinfang Nie  ; Shumin Xiao  ; Dawei Lu   ; Junfeng Wang   ; Qinghai Song  

 Check for updates

Appl. Phys. Rev. 12, 031301 (2025)

<https://doi.org/10.1063/5.0262377>



View
Online

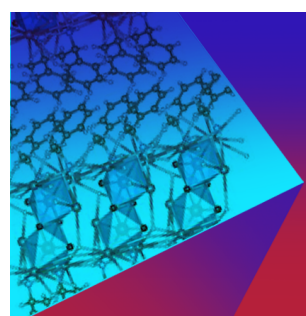


Export
Citation

Articles You May Be Interested In

Two-scale structure of the current layer controlled by meandering motion during steady-state collisionless driven reconnection

Phys. Plasmas (July 2004)



Applied Physics Reviews
Special Topics
Open for Submissions

Submit Today

 AIP
Publishing

Silicon carbide: A promising platform for scalable quantum networks

Cite as: Appl. Phys. Rev. **12**, 031301 (2025); doi: [10.1063/5.0262377](https://doi.org/10.1063/5.0262377)

Submitted: 1 February 2025 · Accepted: 12 June 2025 ·

Published Online: 1 July 2025



Yu Zhou,^{1,2,a)} **Junhua Tan**,¹ **HaiBo Hu**,^{1,3} **Sikai Hua**,¹ **Chunhui Jiang**,¹ **Bo Liang**,¹ **Tongyuan Bao**,¹ **Xinfang Nie**,⁴ **Shumin Xiao**,^{1,2,3,5} **Dawei Lu**,^{4,a)} **Junfeng Wang**,^{6,a)} and **Qinghai Song**,^{1,2,3,5,a)}

AFFILIATIONS

¹ Ministry of Industry and Information Technology Key Lab of Micro-Nano Optoelectronic Information System, Guangdong Provincial Key Laboratory of Semiconductor Optoelectronic Materials and Intelligent Photonic Systems, Harbin Institute of Technology, Shenzhen 518055, People's Republic of China

² Quantum Science Center of Guangdong-HongKong-Macao Greater Bay Area (Guangdong), Shenzhen 518045, People's Republic of China

³ Pengcheng Laboratory, Shenzhen 518055, People's Republic of China

⁴ Department of Physics, State Key Laboratory of Quantum Functional Materials, and Guangdong Basic Research Center of Excellence for Quantum Science, Southern University of Science and Technology, Shenzhen 518055, China

⁵ Collaborative Innovation Center of Extreme Optics, Shanxi University, Taiyuan 030006, Shanxi, People's Republic of China

⁶ College of Physics, Sichuan University, Chengdu 610065, People's Republic of China

Note: This paper is part of the Special Topic, Quantum Light.

^{a)} Authors to whom correspondence should be addressed: zhouyu2022@hit.edu.cn; ludw@sustech.edu.cn; jfwang@scu.edu.cn; and qinghai.song@hit.edu.cn

ABSTRACT

Quantum networks based on solid-state spin defects present a transformative approach to secure communication and distributed quantum computing, utilizing quantum entanglement and coherent spin-photon interfaces. Silicon carbide (SiC) stands out as a compelling material platform due to its unique combination of a wide bandgap, high optical nonlinearity, CMOS-compatible fabrication, and controllable spin-active defects. These intrinsic properties facilitate efficient photon emission, robust spin coherence at both room and cryogenic temperatures, and integration with photonic nanostructures. Recent advancements in defect engineering and micro-nanophotonics have unlocked the potential of SiC quantum nodes, which feature electron-nuclear spin systems for high-fidelity quantum operations and long-lived quantum memories. Key steps such as single-shot readout and spin-photon entanglement have been successfully demonstrated, bringing SiC closer to a real quantum network platform. This review offers a comprehensive overview of the advancements in SiC-based quantum networks, encompassing key aspects such as defect fabrication methodologies, optimization of spin-photon interfaces, and strategies for photonic integration. Additionally, it examines the existing challenges and outlines promising future directions in this rapidly evolving field.

Published under an exclusive license by AIP Publishing. <https://doi.org/10.1063/5.0262377>

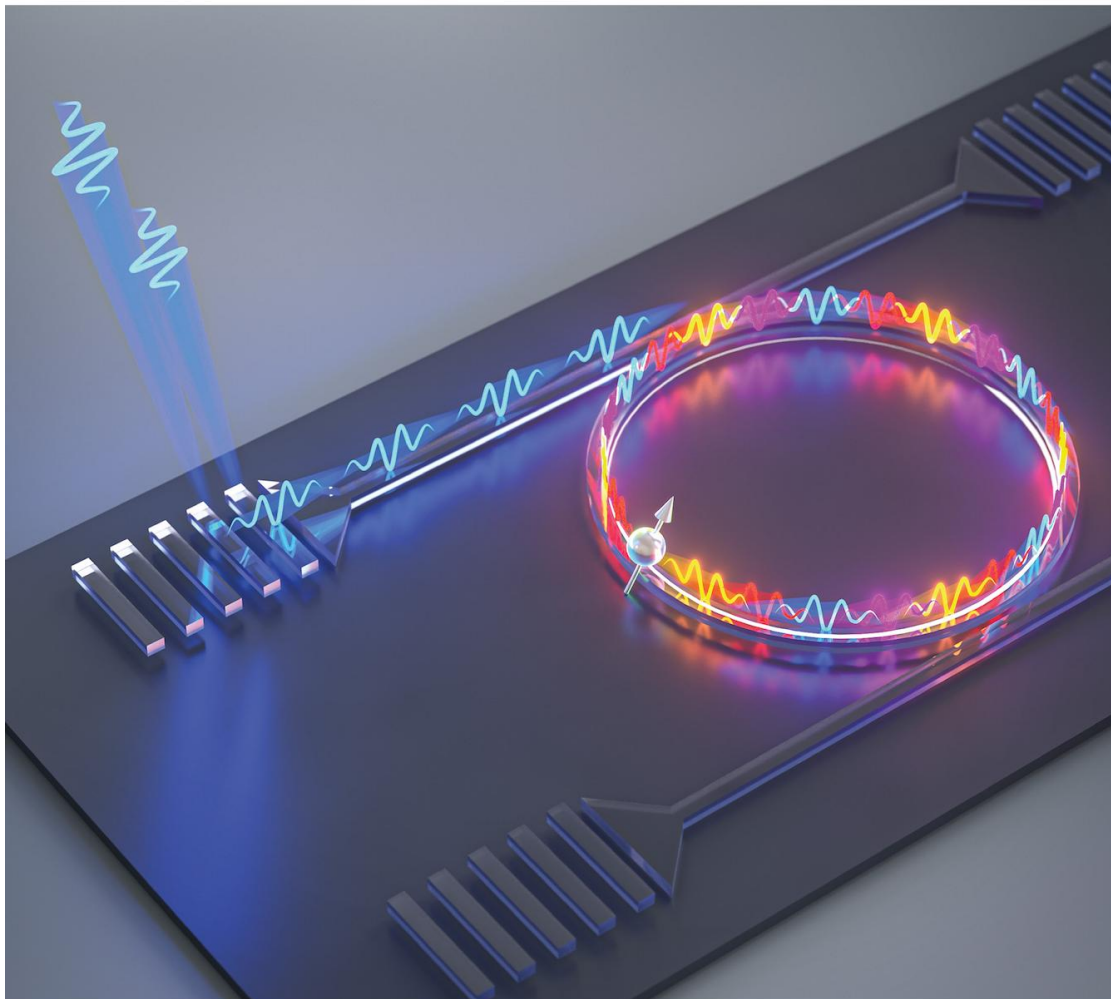
02 July 2025 01:35:58

TABLE OF CONTENTS

I. INTRODUCTION.....	2	A. Spins in SiC	4
II. FABRICATION TECHNIQUES OF SPIN DEFECTS IN SiC	3	1. Electron spin	4
A. Electron or neutron irradiation.....	3	2. Nuclear spin.....	7
B. Ion implantation	3	B. Photons in SiC.....	7
C. Focused ion beam	4	1. Wavelength tuning and linewidth reduction ..	7
D. Laser writing	4	2. Wavelength conversion	8
III. SPIN AND PHOTONS OF SPIN DEFECTS IN SiC...	4	IV. SPIN-PHOTON INTERFACE	9
		A. Single-shot readout	9
		B. Spin-photon interface in SiC.....	9



JUNE 2025
VOLUME 12
NUMBER 6
pubs.acs.org/photonics



ACS Publications
Most Trusted. Most Cited. Most Read.

www.acs.org

Tunable Cavity Coupling to Spin Defects in a 4H-Silicon-Carbide-On-Insulator Platform

Tongyuan Bao,[○] Qi Luo,[○] Ailun Yi,[○] Bo Liang, Yao Zhang, Hai-Bo Hu, Shen Lai, Zhengtong Liu, Shumin Xiao, Xin Ou,* Yu Zhou,* and Qinghai Song*



Cite This: *ACS Photonics* 2025, 12, 2988–2996



Read Online

ACCESS |

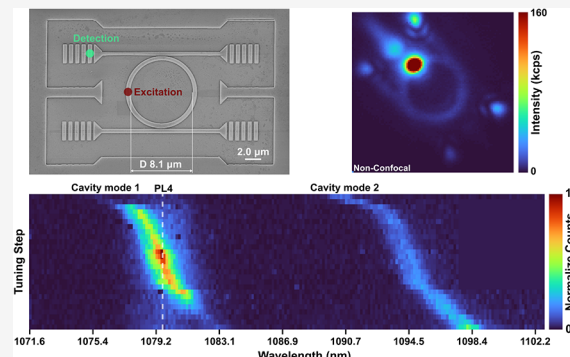
Metrics & More

Article Recommendations

Supporting Information

ABSTRACT: Silicon carbide (SiC) has attracted significant attention as a promising quantum material due to its ability to host long-lived, optically addressable color centers with solid-state photonic interfaces. The CMOS compatibility of 4H-SiCOI (silicon-carbide-on-insulator) makes it an ideal platform for integrated quantum photonic devices and circuits. While microring cavities have been extensively studied in SiC and other materials, the integration of 4H-SiC spin defects into these critical structures, along with continuous mode tunability, remains unexplored. In this work, we demonstrate the integration of PL4 divacancy spin defects into tunable microring cavities in scalable thin-film 4H-SiC nanophotonics. Comparing on- and off-resonance conditions, we observed an enhancement of the Purcell factor by approximately 5.0. This enhancement effectively confined coherent photons within the coupled waveguide, leading to a 2-fold increase in the ODMR (optically detected magnetic resonance) contrast and coherent control of PL4 spins. These advancements lay the foundation for developing SiC-based quantum photonic circuits.

KEYWORDS: silicon carbide, quantum photonic devices, spin defects



INTRODUCTION

Long-lived and optically addressable spin defects in silicon carbide^{1,2} are emerging as a promising quantum candidate due to their robustness, versatile control,^{3–6} and developed readout methods.^{7,8} One advantage of silicon carbide compared to diamond is its compatibility with complementary metal-oxide-semiconductor (CMOS) fabrication technology.^{9,10} This makes 4H-SiCOI (silicon-carbide-on-insulator) a promising platform for advancing integrated quantum photonic devices and circuits.^{9–13} However, leveraging 4H-SiCOI for the continued scaling up quantum networks presents a significant challenge: achieving precise and continuous tunability of the interaction between photonic cavities and spin defects.^{12,14–17} This is especially important for enhancing zero-phonon line (ZPL) emissions over those in the phonon sideband. Boosting emissions into the ZPL is essential for achieving key milestones in the construction of quantum networks, such as single-shot readout,^{1,7,18} spin-photon entanglement,^{19,20} and heralded between remote nodes,^{21–23} where coherent and indistinguishable photons are needed.

Cavity-coupled color centers have been demonstrated using 4H-SiC 1D nanobeam cavities created through bulk carving techniques,^{14,15,24} and 3C-SiC 2D photonic cavities.²⁵ Advances in quantum-grade 4H-SiCOI thin films¹² have opened new opportunities for photonic integration. For instance, suspended 4H-SiC-on-insulator (SiCOI) microdisk

resonators coupled to V_{Si} color centers demonstrate progress in this material via undercut techniques.²⁶ The microring cavity, a key element in nonlinear optics and photonics,^{27,28} offers several advantages: its in-plane geometry allows seamless coupling to waveguides through evanescent fields, enabling low-loss on-chip photon routing and modular interconnects for scalable architectures. Its nonsuspended structure ensures mechanical stability during fabrication. Notably, the CMOS-compatible fabrication process allows for wafer-scale integration with established photonic platforms, reducing costs and complexity for mass production. While microring cavities have been fabricated in SiC^{12,29} and other materials,^{30,31} the integration of 4H-SiC spin defects into this critical structure, along with continuous mode tunability, has not yet been achieved. In this work, we address this gap by demonstrating the monolithic integration of PL4 divacancy spins into tunable microring resonators on thin-film 4H-SiC, laying the groundwork for developing SiC-based quantum photonic circuits.

Received: December 23, 2024

Revised: April 15, 2025

Accepted: April 15, 2025

Published: April 22, 2025



光子学研究 ISSN 2327-9125 CN 31-2126/O4



PHOTONICS Research

Volume 12 | Issue 8 | August 2024

All-optical Nanoscale Thermometry

PAGE 1696



CHINESE
LASER
PRESS
中国激光杂志社



2009-2024

OPTICA
PUBLISHING GROUP

PHOTONICS Research

All-optical nanoscale thermometry with silicon carbide color centers

CHENGYING LIU,^{1,†} HAIBO HU,^{1,2,†} ZHENGTONG LIU,² SHUMIN XIAO,^{1,2} JUNFENG WANG,^{5,6} YU ZHOU,^{1,3,*} AND QINGHAI SONG^{1,3,4,7} 

¹Ministry of Industry and Information Technology Key Laboratory of Micro-Nano Optoelectronic Information System, Guangdong Provincial Key Laboratory of Semiconductor Optoelectronic Materials and Intelligent Photonic Systems, Harbin Institute of Technology, Shenzhen 518055, China

²Pengcheng Laboratory, Shenzhen 518055, China

³Quantum Science Center of Guangdong-Hong Kong-Macao Greater Bay Area, Shenzhen-Hong Kong International Science and Technology Park, Shenzhen 518045, China

⁴Collaborative Innovation Center of Extreme Optics, Shanxi University, Taiyuan 030006, China

⁵College of Physics, Sichuan University, Chengdu 610065, China

⁶e-mail: jfwang@scu.edu.cn

⁷e-mail: qinghai.song@hit.edu.cn

[†]The authors contributed equally to this work.

*Corresponding author: zhouyu2022@hit.edu.cn

Received 11 April 2024; revised 10 June 2024; accepted 15 June 2024; posted 18 June 2024 (Doc. ID 525971); published 1 August 2024

All-optical thermometry plays a crucial role in precision temperature measurement across diverse fields. Quantum defects in solids are one of the most promising sensors due to their excellent sensitivity, stability, and biocompatibility. Yet, it faces limitations, such as the microwave heating effect and the complexity of spectral analysis. Addressing these challenges, we introduce a novel approach to nanoscale optical thermometry using quantum defects in silicon carbide (SiC), a material compatible with complementary metal-oxide-semiconductor (CMOS) processes. This method leverages the intensity ratio between anti-Stokes and Stokes emissions from SiC color centers, overcoming the drawbacks of traditional techniques such as optically detected magnetic resonance (ODMR) and zero-phonon line (ZPL) analysis. Our technique provides a real-time, highly sensitive (1.06 K^{-1}), and diffraction-limited temperature sensing protocol, which potentially helps enhance thermal management in the future miniaturization of electronic components. © 2024 Chinese Laser Press

<https://doi.org/10.1364/PRJ.525971>

1. INTRODUCTION

The field of nanoscale optical thermometry has experienced significant growth recently, becoming crucial in various areas such as materials science [1], biophotonics [2,3], and semiconductor engineering [4]. Among the numerous thermal sensors, such as quantum dots [5,6], fluorescent dyes [7], and nanoparticles [8], quantum defects in solids [9] emerge as particularly noteworthy. Their appeal lies in their robustness, biocompatibility, and wide operating temperature range, maintaining performance even under harsh environmental conditions, e.g., nitrogen-vacancy (NV) centers [10–12] and silicon-vacancy (SiV) centers [9] in nanodiamonds. Most demonstrated thermometry using these defects has relied on techniques such as microwave-involved optically detected magnetic resonance (ODMR) [3] or analyzing the photon properties of zero-phonon lines (ZPLs) [9,13]. However, ODMR methods face challenges due to microwave-induced heating [14] and magnetic field noise sensitivity [15]. Meanwhile, ZPL-based approaches require constant spectral

analysis, limiting their application in terms of speed and temperature resolution.

An emerging all-optical technique that measures the intensity ratio between anti-Stokes and Stokes emissions from color centers [16–19] is gaining prominence for its real-time capabilities, high-temperature sensitivity, and spatial resolution at the diffraction limit. As electronic components continue to miniaturize, efficient thermal management is essential to avert heat accumulation that could compromise device integrity. The integration of this thermometry into semiconductor processes, particularly with CMOS compatibility, heralds new possibilities in computing and electronics, positioning nanoscale optical thermometry as a cornerstone for forthcoming technological and medical breakthroughs [2]. This work demonstrates all-optical thermometry using quantum defects in CMOS-compatible material silicon carbide, circumventing the complexities of dual-laser excitation [17] and spectral analysis [9], simplifying the immediate temperature sensing process. The use of SiC quantum defects not only enhances the

Enhancement of silicon vacancy fluorescence intensity in silicon carbide using a dielectric cavity

QI-CHENG HU,^{1,†} JI XU,^{2,†} QIN-YUE LUO,¹ HAI-BO HU,² PEI-JIE GUO,¹ CHENG-YING LIU,²
SHUANG ZHAO,¹ YU ZHOU,^{2,3,4} AND JUN-FENG WANG^{1,*}

¹College of Physics, Sichuan University, Chengdu 610065, China

²Ministry of Industry and Information Technology Key Lab of Micro-Nano Optoelectronic Information System, Guangdong Provincial Key Laboratory of Semiconductor Optoelectronic Materials and Intelligent Photonic Systems, Harbin Institute of Technology, Shenzhen, 518055, China

³Quantum Science Center of Guangdong-Hong Kong-Macao Greater Bay Area (Guangdong), Shenzhen 518045, China

⁴zhouyu2022@hit.edu.cn

† These authors contributed equally to this Letter.

*jfwang@scu.edu.cn

Received 4 March 2024; revised 16 April 2024; accepted 29 April 2024; posted 29 April 2024; published 22 May 2024

Over the past decades, spin qubits in silicon carbide (SiC) have emerged as promising platforms for a wide range of quantum technologies. The fluorescence intensity holds significant importance in the performance of quantum photonics, quantum information process, and sensitivity of quantum sensing. In this work, a dual-layer Au/SiO₂ dielectric cavity is employed to enhance the fluorescence intensity of a shallow silicon vacancy ensemble in 4H-SiC. Experimental results demonstrate an effective fourfold augmentation in fluorescence counts at saturating laser power, corroborating our theoretical predictions. Based on this, we further investigate the influence of dielectric cavities on the contrast and linewidth of optically detected magnetic resonance (ODMR). There is a 1.6-fold improvement in magnetic field sensitivity. In spin echo experiments, coherence times remain constant regardless of the thickness of dielectric cavities. These experiments pave the way for broader applications of dielectric cavities in SiC-based quantum technologies. © 2024 Optica Publishing Group

<https://doi.org/10.1364/OL.522770>

Introduction. In recent years, color centers in SiC have attracted considerable attention in quantum technologies [1–11]. Particularly, the silicon vacancy in SiC has been widely used in various quantum technologies due to its exceptional properties such as near-infrared fluorescence and long coherence time [3,8,10]. The silicon vacancy is a spin qubit ($S = 3/2$) consisting of a missing silicon atom in 4H or 6H SiC lattices [3,7,8,10]. However, the missing silicon atom may be on hexagonal h-lattice points or quasi-cubic k-lattice points, which corresponds to two types of silicon vacancies, V1 and V2. The zero phonon lines of V1 and V2 are 861 nm and 915 nm, respectively. The zero-field splitting (ZFS) 2D of V1 and V2 is 4 MHz and 70 MHz, respectively [3,4,12]. Since the spin state of the V2 centers can be read out at room temperature and the ZFS remains constant as the temperature increases from 20 to 500 K [12,13], a significant portion of the prior research has concentrated on the V2 centers [3,7,8,10].

Therefore, we conduct our study using the V2 center throughout this work. In quantum photonics, the silicon vacancy in SiC has been coupled to various photonics structures, achieving the Purcell enhancement and nonlinear photonics [7,14]. In quantum information processing, the nuclear quantum register has been realized [8]. A high-fidelity spin-photon interface has successfully demonstrated its potential for constructing a scalable quantum network [15]. Furthermore, the utilization of silicon vacancies has been extended to a wide range of quantum sensing applications, such as magnetic field [16–18], temperature [13,19,20], and high-pressure magnetic detection [10]. Particularly, optically detected magnetic resonance (ODMR)-based nanotesla magnetometry has been achieved by utilizing a silicon vacancy ensemble generated through the thermal quenching method [18].

The fluorescence intensity is important for various quantum technologies. However, the maximum count achievable from a single silicon vacancy is only approximately 10 kcps, limiting its potential applications in quantum information [3]. Consequently, several approaches have been devised to augment the counts. Recently, the scalable-fabricated solid immersion lenses (SILs) have enhanced the counts by 2–4 times [3,21,22]. Scalable 800 nm high nanopillars with diameters ranging from 400 to 1400 nm enhance the counts by about three times [23]. Photonic crystal cavities have been employed to achieve an 80-fold Purcell enhancement of the ZPL of silicon vacancies [7,14,24]. However, all the methods require intricate micro-nanofabrication technologies, and achieving alignment between the silicon vacancy and the optimal mode position of photonic structures remains a challenging task [3,14,23–26]. The aforementioned points induce the non-ideal enhancement.

In this work, we achieve a significant increase in the counts of a shallow silicon vacancy ensemble in 4H-SiC by implementing a two-layer Au/SiO₂ dielectric cavity [27–29]. The counts exhibit variations depending on the thickness of SiO₂ films, with an optical fourfold enhancement observed at 20 nm at the saturating laser power. Based on this, we conduct a comparison of the ODMR between a bare SiC and a dielectric cavity, under

ARTICLE

Received 30 Jun 2016 | Accepted 30 Dec 2016 | Published 20 Feb 2017

DOI: 10.1038/ncomms14451

OPEN

Coherent control of a strongly driven silicon vacancy optical transition in diamond

Yu Zhou¹, Abdullah Rasmita¹, Ke Li¹, Qihua Xiong¹, Igor Aharonovich^{2,3} & Wei-bo Gao¹

The ability to prepare, optically read out and coherently control single quantum states is a key requirement for quantum information processing. Optically active solid-state emitters have emerged as promising candidates with their prospects for on-chip integration as quantum nodes and sources of coherent photons connecting these nodes. Under a strongly driving resonant laser field, such quantum emitters can exhibit quantum behaviour such as Autler-Townes splitting and the Mollow triplet spectrum. Here we demonstrate coherent control of a strongly driven optical transition in silicon vacancy centre in diamond. Rapid optical detection of photons enabled the observation of time-resolved coherent Rabi oscillations and the Mollow triplet spectrum. Detection with a probing transition further confirmed Autler-Townes splitting generated by a strong laser field. The coherence time of the emitted photons is comparable to its lifetime and robust under a very strong driving field, which is promising for the generation of indistinguishable photons.

¹ Division of Physics and Applied Physics, School of Physical and Mathematical Sciences, Nanyang Technological University, 21 Nanyang Link, Singapore 637371, Singapore. ² School of Mathematical and Physical Sciences, University of Technology Sydney, Ultimo, New South Wales 2007, Australia. ³ Faculty of Science, Institute of Biomedical Materials and Devices (IBMD), University of Technology Sydney, Ultimo, New South Wales 2007, Australia. Correspondence and requests for materials should be addressed to I.A. (email: Igor.Aharonovich@uts.edu.au) or to W.-b.G. (email: wbgao@ntu.edu.sg.).

Coherent control of atom-photon interfaces is vital in the realization of quantum information protocols. In particular, the interface between solid-state qubits and photons is a promising candidate for practical and scalable quantum technologies^{1–5}. Different types of defects in solids have been studied so far and many of them show excellent optical or spin properties to be proper quantum qubit candidates. Among others, the nitrogen vacancy (NV) centres in diamond have achieved partial success in spin-photon interface and spin–spin entanglement mediated by photons^{1,2}. However, despite the long spin coherence times of the NV, the defect suffers from low percentage (3–5%) of the total emission into its weak zero phonon line (ZPL) and from strong inhomogeneous broadening. Recently, increased efforts have been made to identify other solid-state qubits with improved inherent properties. The silicon vacancy (SiV) centre in diamond is one potential candidate, with ~70% of the photons emitted into the ZPL^{6,7}. Different SiV defects exhibit intrinsically identical spectral properties in low-strain bulk diamond^{8,9} and nearly transform-limited linewidth^{9–12}. SiV spin coherence times are in the range of ~40 ns at cryogenic (4 K) temperatures^{13,14}. It is important to note that the coherence times are only limited by spin relaxation time and are estimated to increase dramatically at lower temperatures¹⁵. As a result, the SiV defect has become a promising candidate to be a key building block for quantum information processing.

Towards this goal, preparation and coherent control of the emitted photons from SiV is a prerequisite. For a two-level system under strong pumping resonant field excitation, state population will oscillate between the ground and the excited states, also known as Rabi oscillations. In the frequency domain, the emission under continuous wave (cw) laser excitation will exhibit the Mollow triplet spectrum¹⁶, which is a hallmark for quantum coherent control and enables a robust approach to generate single photons with detuned frequency from the resonance^{17–25}.

In this work, we demonstrate coherent control of a strongly driven single SiV defect in diamond. In particular, we observe Rabi oscillations with fast photon detection using both a nanosecond laser pulse and a cw laser field. A Fourier transform of the time-resolved detection combined with laser detuning results in an observation of the Mollow triplet spectrum. In the frequency domain, the Autler splitting has been confirmed by a Λ-shape energy scheme^{13,14}. In the above measurements, photon coherence, which is critical for photon interference in building a quantum network, has been characterized in both the low- and the high-power regime.

Results

Transitions in a single SiV in diamond. The SiV defect consists of an interstitial silicon atom, neighbouring two vacancies along a [111] crystallographic axis in diamond²⁶, as shown in Fig. 1a. The defect is negatively charged and has a D_{3d} symmetry, which is inert to strain and fluctuating electric fields^{27–29}. The electronic structure and optical transitions of the negatively charged SiV in diamond have been characterized in detail recently^{28–30}. Both ground and excited states of the SiV ZPL are split due to spin-orbit coupling, resulting in four lines at cryogenic temperature as shown in Fig. 1b (black solid lines). In our experiment, the transitions are successfully identified by scanning a resonant laser and recording the photoluminescence at the same time (see Supplementary Fig. 1). For the current work, coherent control is performed on transition C as marked in Fig. 1b. Transition C is associated with the lower energy levels in both the excited state and ground state in SiV. It does not suffer from fast relaxation from the upper branches of the energy levels, therefore

offering a better count rate and longer coherence times compared with the A, B and D transitions. By resonantly exciting transition C and collecting the photons at the phonon sideband above 750 nm, a narrow linewidth of 219 MHz at saturation power is achieved (Fig. 1c). The linewidth without power broadening is 154 MHz, close to the transform-limited linewidth of 86 MHz, calculated from a direct lifetime measurement that is shown in Fig. 1d.

Time-resolved Rabi oscillations. We first demonstrate real-time observation of the time-resolved Rabi oscillations measured with a superconducting detector with a short jitter time. In the time domain, a strong resonant cw laser coupled to a two-level system yields oscillations of the excited state population and can be described by $\sin^2(\Omega_g t/2)$, where $\Omega_g = \sqrt{\Delta^2 + \Omega^2}$, where Δ is the laser detuning, $\Omega = \mu E/\hbar$ is the bare Rabi frequency, μ is the optical transition dipole moment and E is the driving field amplitude. In the frequency domain, the physics model can be best demonstrated with a dressed state as shown in Fig. 1b (red dashed lines). Under a strong laser field, the ground state and excited state will split (Autler-Townes splitting) into two states separated by an energy $\Omega_g = \sqrt{\Delta^2 + \Omega^2}$. Two frequencies of the emission from four transitions are degenerate and therefore the dressed state will result in an emission pattern with three Lorentzian lines with centre frequency $\nu_0 + \Delta$ and $\nu_0 + \Delta \pm \Omega_g$.

In our experiment, a 5 ns laser pulse is used to excite a single SiV centre. The emitted photons are collected and analysed with a time-correlated single-photon counting system (see Methods). As shown in Fig. 2a, the Rabi oscillations are clearly observed with a shorter oscillation period corresponding to a higher excitation power. The curves are fitted with the theoretical value of excited state population, which can be expressed as (up to a displacement time dt)¹⁹

$$P = 1 - e^{-\eta|\tau|} \left(\cos(\mu|\tau|) + \frac{\eta}{\mu} \sin(\mu|\tau|) \right) \quad (1)$$

Here $\eta = 1/2T_1 + 1/2T_2$ and $\mu = \sqrt{\Omega_g^2 + (1/2T_1 - 1/2T_2)^2}$, where T_1 and T_2 are the lifetime and the photon coherence time, respectively. In the fitting, T_2 and Ω_g are used as free parameters, while the measured T_1 value is 1.85 ± 0.02 ns. The extracted Rabi frequency is linearly proportional to the square root of the excitation power, confirming the Rabi oscillation behaviour (Fig. 2b). Average value of T_2 is calculated to be 1.62 ns, smaller than the ideal value $2T_1 = 3.7$ ns. This is likely to be due to the pure dephasing of the excited state. More importantly, as shown in Fig. 2c, the value of T_2 stays above 1.3 ns even with a Rabi frequency of 12 GHz, corresponding to 300 times of saturation power. This shows that no apparent excitation induced dephasing is observed. This can be partially explained by the weak electron-phonon coupling of the SiV and the reduced sensitivity to fluctuating electric fields within the diamond lattice^{8–12}. Robust T_2 , combined with the frequency stability and efficient generation of SiV single photons, shows the feasibility of SiV as an efficient and coherent single photon source.

The plot of the time-dependent fluorescence intensity profile as a function of laser detuning is shown in Fig. 2d. With the laser detuning, the oscillation frequency is increased to the generalized Rabi frequency $\sqrt{\Omega^2 + \Delta^2}$. To best illustrate this phenomenon, a Fourier transform of each curve is taken and the frequency components are shown as a function of the laser detuning. Three peaks corresponding to the three frequency components of the Mollow triplet can clearly be seen. The dashed lines in Fig. 2e corresponds to the theoretical centre frequency $\nu_0 + \Delta \pm \sqrt{\Omega^2 + \Delta^2}$ with Ω extracted when the laser detuning is 0.

fused silica etalon (FSR 30 GHz, Finesse ~ 20) and after filtering, the picosecond laser was narrowed to 1.65 GHz, which is sufficient to avoid cross-excitation. In the Ramsey experiment, the laser beam was split by a 50:50 beam splitter. One arm of the beam was delayed by moving the retro-reflector (Thorlabs PS976/M) and then combined with the other undelayed beam using another 50:50 beam splitter.

Diamond growth. The diamond sample was grown using a microwave plasma chemical vapour deposition technique. Detonation nanodiamonds (4–6 nm) were dispersed on a silicon substrate and used as seeds for the diamond growth. The growth condition was 60 Torr, 950 W. The final size of the nanodiamonds was several hundreds of nanometres.

Note added. In preparation of this manuscript, we noted a paper reporting a complementary method for measuring the Rabi oscillations³⁷.

Data availability. All summary data are included in the manuscript and Supplementary Information. Requests for more detailed data collected for this study are available from the corresponding author on request.

References

- Togan, E. *et al.* Quantum entanglement between an optical photon and a solid-state spin qubit. *Nature* **466**, 730–734 (2010).
- Bernien, H. *et al.* Heralded entanglement between solid-state qubits separated by three metres. *Nature* **497**, 86–90 (2013).
- Gao, W. B., Fallahi, P., Togan, E., Miguel-Sanchez, J. & Imamoglu, A. Observation of entanglement between a quantum dot spin and a single photon. *Nature* **491**, 426–430 (2012).
- De Greve, K. *et al.* Quantum-dot spin-photon entanglement via frequency downconversion to telecom wavelength. *Nature* **491**, 421–425 (2012).
- Schaibley, J. R. *et al.* Demonstration of quantum entanglement between a single electron spin confined to an InAs quantum dot and a photon. *Phys. Rev. Lett.* **110**, 167401 (2013).
- Neu, E. *et al.* Single photon emission from silicon-vacancy colour centres in chemical vapour deposition nano-diamonds on iridium. *New J. Phys.* **13**, 025012 (2011).
- Collins, A. T., Allers, L., Wort, C. J. & Scarsbrook, G. A. The annealing of radiation damage in the Beers colourless CVD diamond. *Diamond Related Mater.* **3**, 932 (1994).
- Rogers, L. J. *et al.* Multiple intrinsically identical single-photon emitters in the solid state. *Nat. Commun.* **5**, 4739 (2014).
- Evans, R. E., Sipahigil, A., Sukachev, D. D., Zibrov, A. S. & Lukin, M. D. Narrow-linewidth homogeneous optical emitters in diamond nanostructures via silicon ion implantation. *Phys. Rev. Appl.* **5**, 044010 (2016).
- Li, K., Zhou, Y., Rasmita, A., Aharonovich, I. & Gao, W. B. Nonblinking emitters with nearly lifetime-limited linewidths in CVD nanodiamonds. *Phys. Rev. Appl.* **6**, 024010 (2016).
- Jantzen, U. *et al.* Nanodiamonds carrying silicon-vacancy quantum emitters with almost lifetime-limited linewidths. *New J. Phys.* **18**, 073036 (2016).
- Sipahigil, A. *et al.* Indistinguishable photons from separated silicon-vacancy centers in diamond. *Phys. Rev. Lett.* **113**, 113602 (2014).
- Rogers, L. J. *et al.* All-optical initialization, readout, and coherent preparation of single silicon-vacancy spins in diamond. *Phys. Rev. Lett.* **113**, 263602 (2014).
- Pingault, B. *et al.* All-optical formation of coherent dark states of silicon-vacancy spins in diamond. *Phys. Rev. Lett.* **113**, 263601 (2014).
- Jahnke, K. D. *et al.* Electron-phonon processes of the silicon-vacancy centre in diamond. *New J. Phys.* **17**, 4 (2015).
- Mollow, B. R. Power spectrum of light scattered by two-level systems. *Phys. Rev.* **188**, 1969–1975 (1969).
- Wu, F. Y., Grove, R. E. & Ezekiel, S. Investigation of the spectrum of resonance fluorescence by a monochromatic field. *Phys. Rev. Lett.* **35**, 1426–1429 (1975).
- Wrigge, G. *et al.* Efficient coupling of photons to a single molecule and the observation of its resonance fluorescence. *Nat. Phys.* **4**, 60–66 (2007).
- Batalov, A. *et al.* Temporal coherence of photons emitted by single nitrogen-vacancy defect centers in diamond using optical Rabi-oscillations. *Phys. Rev. Lett.* **100**, 77401 (2008).
- Robledo, L., Bernien, H., van Weperen, I. & Hanson, R. Control and coherence of the optical transition of single nitrogen vacancy centers in diamond. *Phys. Rev. Lett.* **105**, 177403 (2010).
- Stievater, T. H. *et al.* Rabi oscillations of excitons in single quantum dots. *Phys. Rev. Lett.* **87**, 133603 (2001).
- Xu, X. *et al.* Coherent optical spectroscopy of a strongly driven quantum dot. *Science* **317**, 929–932 (2007).
- Muller, A. *et al.* Resonance fluorescence from a coherently driven semiconductor quantum dot in a cavity. *Phys. Rev. Lett.* **9**, 187402 (2007).
- Flagg, E. B. *et al.* Resonantly driven coherent oscillations in a solid-state quantum emitter. *Nat. Phys.* **5**, 203–207 (2009).
- Vamivakas, N. A. *et al.* Spin-resolved quantum-dot resonance fluorescence. *Nat. Phys.* **5**, 198–202 (2009).
- Goss, J. P., Jones, R., Breuer, S. J., Briddon, P. R. & Oberg, S. The twelve-line 1.682 eV luminescence center in diamond and the vacancy-silicon complex. *Phys. Rev. Lett.* **77**, 3041 (1996).
- Goss, J. P., Briddon, P. R. & Shaw, M. J. Density functional simulations of silicon-containing point defects in diamond. *Phys. Rev. B* **76**, 075204 (2007).
- Rogers, L. J. *et al.* Electronic structure of the negatively charged silicon-vacancy center in diamond. *Phys. Rev. B* **89**, 235101 (2014).
- Hepp, C. *et al.* Electronic structure of the silicon vacancy color center in diamond. *Phys. Rev. Lett.* **112**, 036405 (2014).
- Muller, T. *et al.* Optical signatures of silicon-vacancy spins in diamond. *Nat. Commun.* **5**, 3328 (2014).
- Sipahigil, A. *et al.* An integrated diamond nanophotonics platform for quantum optical networks. *Science* **354**, 847–850 (2016).
- Ulhaq, A. *et al.* Cascaded single-photon emission from the Mollow triplet sidebands of a quantum dot. *Nat. Photonics* **6**, 238–242 (2012).
- Kim, H., Shen, T., Roy-Choudhury, K., Solomon, G. S. & Waks, E. Resonant interactions between a mollow triplet sideband and a strongly coupled cavity. *Phys. Rev. Lett.* **113**, 027403 (2014).
- Loncar, M. & Faraon, A. Quantum photonic networks in diamond. *MRS Bull.* **38**, 144 (2013).
- Faraon, A. *et al.* Coupling of nitrogen-vacancy centers to photonic crystal cavities in monocrystalline diamond. *Phys. Rev. Lett.* **109**, 033604 (2012).
- Quang, T. & Freedhoff, H. Atomic population inversion and enhancement of resonance fluorescence in a cavity. *Phys. Rev. A* **47**, 2285–2292 (1993).
- Becker, J. N. *et al.* Ultrafast all-optical coherent control of single silicon vacancy colour centres in diamond. *Nat. Commun.* **7**, 13512 (2016).

Acknowledgements

We thank Christoph Becher for discussion. We acknowledge the support from the Singapore National Research Foundation through a Singapore 2015 NRF fellowship grant (NRF-NRFF2015-03) and its Competitive Research Program (CRP Award Number NRF-CRP14-2014-02), and Astar QTF project. I.A. is the recipient of an Australian Research Council Discovery Early Career Research Award (Project Number DE130100592). Partial funding for this research was provided by the Air Force Office of Scientific Research, United States Air Force (grant FA2386-15-1-4044). Q.X. gratefully thanks the Singapore National Research Foundation via Investigatorship award (NRF-NRFI2015-03) and the Ministry of Education for an AcRF Tier2 grant (MOE2012-T2-2-086).

Author contributions

Y.Z. and W.-b.G. designed the experiment. Y.Z., A.R., K.L., Q.H.X. and W.-b.G. built the optical set-up and performed the optical measurements. Y.Z., A.R., K.L., Q.H.X., I.A. and W.B.G. wrote the manuscript. A.R. performed the simulations. I.A. grew the sample. All authors contributed to the discussion of the results and to the manuscript.

Additional information

Supplementary Information accompanies this paper at <http://www.nature.com/naturecommunications>

Competing financial interests: The authors declare no competing financial interests.

Reprints and permission information is available online at <http://npg.nature.com/reprintsandpermissions/>

How to cite this article: Zhou, Y. *et al.* Coherent control of a strongly driven silicon vacancy optical transition in diamond. *Nat. Commun.* **8**, 14451 (2017). doi: 10.1038/ncomms14451 (2017).

Publisher's note: Springer Nature remains neutral with regard to jurisdictional claims in published maps and institutional affiliations.



This work is licensed under a Creative Commons Attribution 4.0 International License. The images or other third party material in this article are included in the article's Creative Commons license, unless indicated otherwise in the credit line; if the material is not included under the Creative Commons license, users will need to obtain permission from the license holder to reproduce the material. To view a copy of this license, visit <http://creativecommons.org/licenses/by/4.0/>

ARTICLE

DOI: 10.1038/s41467-018-06605-3

OPEN

Bright room temperature single photon source at telecom range in cubic silicon carbide

Junfeng Wang¹, Yu Zhou¹, Ziyu Wang¹, Abdullah Rasmita¹, Jianqun Yang², Xingji Li², Hans Jürgen von Bardeleben³ & Weibo Gao^{1,4}

Single-photon emitters (SPEs) play an important role in a number of quantum information tasks such as quantum key distributions. In these protocols, telecom wavelength photons are desired due to their low transmission loss in optical fibers. In this paper, we present a study of bright single-photon emitters in cubic silicon carbide (3C-SiC) emitting in the telecom range. We find that these emitters are photostable and bright at room temperature with a count rate of \sim MHz. Altogether with the fact that SiC is a growth and fabrication-friendly material, our result may be relevant for future applications in quantum communication technology.

¹ Division of Physics and Applied Physics, School of Physical and Mathematical Sciences, Nanyang Technological University, Singapore 637371, Singapore.
² School of Materials Science and Engineering, Harbin Institute of Technology, Harbin 150001, China. ³ INSP, Université Pierre et Marie Curie, UMR 7588 au CNRS 4 place Jussieu, 75005 Paris, France. ⁴ The Photonics Institute and Centre for Disruptive Photonic Technologies, Nanyang Technological University, Singapore 637371, Singapore. These authors contributed equally: Junfeng Wang, Yu Zhou. Correspondence and requests for materials should be addressed to X.L. (email: lxj0218@hit.edu.cn) or to H.J.v.B. (email: vonbarde@insp.jussieu.fr) or to W.G. (email: wbgao@ntu.edu.sg)

Single-photon emitters (SPE) are used to generate “flying qubits” and they are critical in many quantum technology protocols such as quantum information processing^{1–4}, quantum simulation^{5–7}, quantum networks, and quantum communications^{8–11}. Especially, in quantum key distribution (QKD), photons are used to send information in a secure way, protected by quantum mechanics¹¹. Despite the fact that most QKD implementations use weak attenuated lasers to simulate SPE, a true SPE is still preferred due to its longer secure distance in theory and therefore its potentially better performance. In previous pioneer works, single-photon quantum cryptography has been demonstrated with photons emitted from a single nitrogen-vacancy center in diamond¹². The difficulty of QKD using true SPE lies on the fact that it is challenging to find a bright, room temperature (RT) SPE working in the telecom range, which is required to minimize the transmission loss in optical fibers.

Extensive efforts have been made to realize telecom-compatible SPE. InAs/InP QDs (quantum dots) present single-photon emission at telecom wavelength¹³ and they have been utilized to realize 120 km QKD¹⁴. However, QDs require operation at cryogenic temperatures, which makes their use experimentally more demanding. Most recently, room temperature SPEs in carbon nanotubes have equally been demonstrated to have emission in the telecom range^{15,16}.

SiC is a wide band gap semiconductor widely used in LED industry. It is also a prominent material in the application of advanced high power, high temperature electronics. In recent years, defects in SiC have attracted increasing attention owing to their magneto-optical properties and the convenience for fabrication and scalability. Different types of SPEs have been discovered in SiC¹⁷, such as carbon antisite–vacancy pair^{18,19}, silicon vacancies^{20–24}, and divacancies^{25–27}. However, those SPEs have emission either in the visible range^{18–24,28} or being weak in the near-infrared range^{25–27}.

In this paper, we present a type of bright (~MHz) single emitters in 3C-SiC, which work at room temperature and emit in the telecom range. The sample we use is high-purity 3C-SiC epitaxy layer grown on a silicon substrate. First, we measured the

photoluminescence (PL) spectrum of different SPEs and find that their fluorescence wavelengths lie in the telecom region. Then we investigated their optical properties: photostability and saturation behavior. Our results show that they have stable count rates of ~MHz at room temperature. Finally, we investigate their polarization properties for both excitation and emission, which demonstrate that these emitters can be treated as almost perfect single dipole. The polarization degree of both excitation and emission can reach up to around 97%. All these properties are highly desired in the QKD protocols with polarization coding scheme.

Results

Single-photon emission. The use of an epitaxial layer ensures a low background level for SPEs detection. Moreover, it provides a natural way to obtain thin membranes for photonics and micromechanics applications rather than the thinning of bulk crystals²⁶. We study the PL property of the emitters in home-made confocal microscopy systems. For the room temperature experiments, a 950 nm diode laser is used to excite the emitters through a high-NA (1.35) oil objective (Nikon). After passing through a 1000-nm dichroic mirror and a 1000-nm long pass filter, the fluorescence from the emitters is collected by a single-mode fiber. The emission is then guided to two channel superconducting single-photon detectors (SSPD, Scontel) in a Hanbury-Brown and Twiss (HBT) set-up. In the cryogenic experiments, we use a closed cycle cryostation (Montana Instruments) combined with a confocal microscopy system with an infrared air objective with NA of 0.65.

Figure 1a shows a confocal scan of the single emitters in an area of $25 \times 25 \mu\text{m}^2$. Four bright SPEs are circled, which are verified by the continuous wave (CW) second-order autocorrelation function measurement using HBT interferometry. Then we continue to study the PL spectrum of the SPEs. As shown in Fig. 1b, the center wavelengths of three representative RT PL spectra are 1085, 1188, and 1250 nm. By measuring the PL spectrum of many SPEs, we find that the center wavelength of

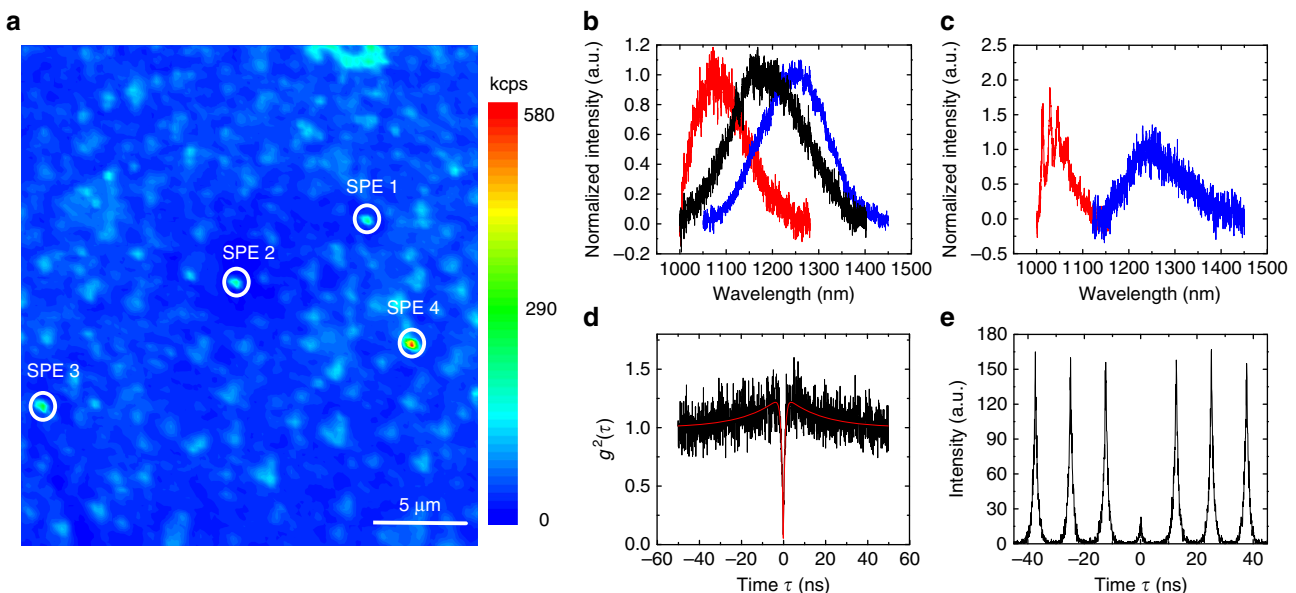


Fig. 1 3C-SiC single-photon emitters. **a** $25 \times 25 \mu\text{m}^2$ confocal map of the SPEs found in 3C-SiC epitaxy layer under 2 mW laser excitation. The scale bar is $5 \mu\text{m}$. SPEs are marked with white circles. **b** Three representative RT PL spectra of the SPEs. **c** Two representative PL spectra of the SPEs at cryogenic temperature (5 K). **d** Second-order autocorrelation function of SPE 4 with $g^2(0) = 0.05 \pm 0.03$ under 0.2 mW continuous wave (CW) laser excitation. The black line is the raw data and red solid line is the fitting with Eq. (1). **e** Second-order autocorrelation function of SPE 4 with $g^2(0) = 0.13 \pm 0.02$ under pulsed laser excitation (50 μW).

MATERIALS SCIENCE

Room temperature solid-state quantum emitters in the telecom range

Yu Zhou,¹ Ziyu Wang,¹ Abdullah Rasmita,¹ Sejeong Kim,² Amanuel Berhane,² Zoltán Bodrog,³ Giorgio Adamo,^{1,4} Adam Gali,^{3,5} Igor Aharonovich,^{2*} Wei-bo Gao^{1,4*}

On-demand, single-photon emitters (SPEs) play a key role across a broad range of quantum technologies. In quantum networks and quantum key distribution protocols, where photons are used as flying qubits, telecom wavelength operation is preferred because of the reduced fiber loss. However, despite the tremendous efforts to develop various triggered SPE platforms, a robust source of triggered SPEs operating at room temperature and the telecom wavelength is still missing. We report a triggered, optically stable, room temperature solid-state SPE operating at telecom wavelengths. The emitters exhibit high photon purity (~5% multiphoton events) and a record-high brightness of ~1.5 MHz. The emission is attributed to localized defects in a gallium nitride (GaN) crystal. The high-performance SPEs embedded in a technologically mature semiconductor are promising for on-chip quantum simulators and practical quantum communication technologies.

INTRODUCTION

In the last decade, SPEs have been explored as key resources for many quantum technologies (1–7), including quantum computation (8), quantum simulation (9–11), quantum metrology (12), and quantum communications (13–15), where the photons are used as “flying qubits”. In linear optical quantum computation, the information is carried by single photons that interact with each other through optical elements and projective measurements (8). In a Boson sampling quantum machine, single photons are used as inputs for a series of interferometers to complete photonic circuits (16). Furthermore, for most of the quantum key distribution (QKD) systems, single photons are the most fundamental building blocks (15). However, because of the lack of a practical ultrabright triggered SPE, current QKD systems widely use weak coherent pulse (from attenuated lasers). In this regard, a true SPE would still be preferred to achieve a longer secure distance and, thus, better performance.

For the above-mentioned applications, the operation wavelength is preferred to be in the telecom range because of its lower attenuation loss in fiber transmission performance as compared to shorter wavelengths. Current solutions for triggered SPEs at this wavelength range mostly rely on a variety of semiconductor quantum dots (QDs). For instance, InAs/InP QDs have single-photon emission at telecom wavelength (17) and have been used to realize 120-km QKD (18), whereas InAs/InGaAs QDs have been used for the generation of entangled photon pairs (19). However, these sources require cryogenic cooling down to liquid helium temperatures, which is not ideal for many scalable and practical devices. In a complementary approach, down-conversion of near-infrared photons to the telecom range was used (20). However, the photon generation is limited by the nonideal conversion efficiency in the nonlinear process. Finally, recent studies of chemically modified

single-walled carbon nanotubes showed optically stable, room temperature (RT) SPEs in the infrared spectral range (1.2 to 1.5 μm) (21).

Here, we report on unprecedented photostable, RT SPEs embedded in a GaN crystal and operating at the telecom range. The SPEs exhibit both excellent purity, with $g^2(0) \sim 0.05$, and a high brightness exceeding 10^6 counts/s. A number of GaN defects ranging from the ultraviolet (UV) to infrared wavelength have been predicted with a density functional study (22). However, most of the experimental studies have been focused on defects in the UV (23) and the visible range (24), whereas emitters in the infrared range remained largely unexplored. Moreover, because nanofabrication procedures with GaN are well established, the discovery of telecom SPEs can be instantly adopted and is highly promising for practical quantum technologies.

RESULTS

Figure 1A shows the GaN crystal structure and an optical image of a typical GaN wafer where SPEs were observed. The studied sample is a 2- μm -thick magnesium (Mg)-doped GaN layer on a 2- μm undoped GaN layer grown on sapphire. We first studied the photoluminescence (PL) spectra of GaN emitters with a home-built confocal scanning setup, where a 950-nm diode laser was used to excite the defect and emission above 1000 nm was collected and guided to a spectrometer or a pair of superconducting detectors in a Hanbury Brown-Twiss (HBT) configuration for photon counting (see Materials and Methods). Emitters are randomly distributed on the GaN substrate, and the confocal PL map around one of the SPEs, named as SPE1, is shown in Fig. 1B as an example. This particular defect emits ~350 kcounts/s at RT. A survey of the sample shows different SPEs with distinct narrowband emission, with zero phonon lines (ZPLs) ranging from 1085 to 1340 nm. The distribution of ZPLs will be discussed below. Examples of three SPEs at RT are given at the lower panel of Fig. 1C, whereas the top panel shows examples of three PL spectra of the SPEs recorded at cryogenic temperature (4 K). At RT, the full width at half maximum (FWHM) of the emitters’ linewidth ranges from 3 nm (ZPL at 1120 nm) to 50 nm (ZPL at 1285 nm) (see fig. S1 for more information). At 4 K, the FWHM of the measured SPEs reduces to a few nanometers but is still broadened because of the coupling to the lattice phonons.

To confirm the nonclassical photon statistics from the studied emitters, we recorded the second-order autocorrelation function $g^{(2)}(\tau)$.

Copyright © 2018
The Authors, some
rights reserved;
exclusive licensee
American Association
for the Advancement
of Science. No claim to
original U.S. Government
Works. Distributed
under a Creative
Commons Attribution
NonCommercial
License 4.0 (CC BY-NC).

¹Division of Physics and Applied Physics, School of Physical and Mathematical Sciences, Nanyang Technological University, Singapore 637371, Singapore. ²Institute of Biomedical Materials and Devices, Faculty of Science, University of Technology Sydney, Ultimo, New South Wales 2007, Australia. ³Wigner Research Centre for Physics, Institute for Solid State Physics and Optics, Hungarian Academy of Sciences, P.O. Box 49, H-1525 Budapest, Hungary. ⁴The Photonics Institute and Centre for Disruptive Photonic Technologies, Nanyang Technological University, Singapore 637371, Singapore. ⁵Department of Atomic Physics, Budapest University of Technology and Economics, Budafoki út 8, H-1111 Budapest, Hungary.

*Corresponding author. Email: igor.aharonovich@uts.edu.au (I.A.); wbgao@ntu.edu.sg (W.-b.G.)

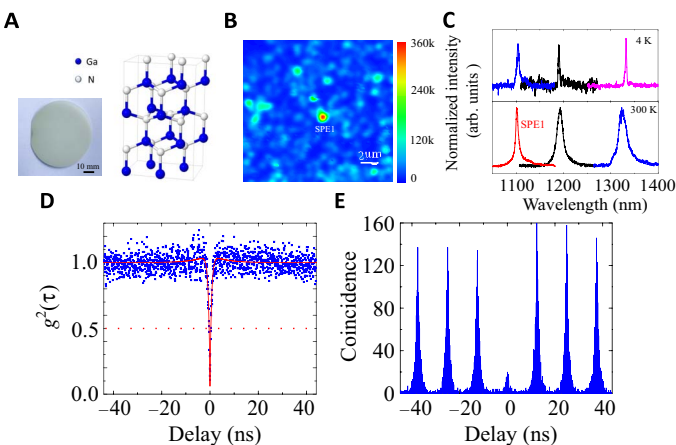


Fig. 1. Infrared single-photon emission in GaN. (A) Schematic illustration of GaN crystal structure and an optical image of the GaN wafer. (B) Confocal PL mapping with a single emitter SPE1 in the center of the map. (C) PL spectra of six infrared emitters, revealing that the PL ranges from 1085 to 1340 nm. PL spectra from three emitters are taken at 4 K (top) and 300 K (bottom), respectively. Note that the emitters at 4 K and RT are different. (D) Second-order correlation measurement of the emission from SPE1 under 950-nm cw laser excitation. The blue dots are the raw data without any background correction, and the red curve is the fitting to a three-level system, yielding $g^2(0) = 0.05 \pm 0.02$. (E) Second-order correlation measurement of SPE1 excited by pulsed laser with a 1-ps pulse width and a 80-MHz repetition rate, yielding $g^2(0) = 0.14 \pm 0.01$. The $g^2(\tau)$ measurements were recorded at RT. arb. units, arbitrary units.

Figure 1D shows the $g^{(2)}(\tau)$ recorded from SPE1 under continuous-wave (cw) laser excitation at RT. The peak at zero delay time indicates that the emission is nonclassical and the source is an SPE. Other emitters have similar properties, and more data can be found in the Supplementary Materials. The data are fit with a three-level model (Eq. 1)

$$g^2(\tau) = 1 - \alpha * \exp(-|\tau|/\tau_1) + \beta * \exp(-|\tau|/\tau_2) \quad (1)$$

where τ_1 and τ_2 are the excited state and the metastable state lifetimes, respectively, and α and β are the fitting parameters. The obtained value at zero time delay $g^2(0)$ is 0.05 ± 0.02 without any background correction, proving that this is one of the purest RT SPEs. The slight deviation from zero is attributed to the background from other defects within the GaN crystal. Furthermore, as shown by the pulsed $g^{(2)}(\tau)$ in Fig. 1E, the SPE can be efficiently triggered. To obtain the $g^{(2)}(\tau)$ in a pulsed regime, we used pulsed laser excitation with a 80-MHz repetition rate and a 1-ps pulse width. The obtained value at zero delay time corresponds to $g^2(0) = 0.14 \pm 0.01$. It is also well below the classical threshold 0.5 for proving SPE. The value of $g^2(0)$ under pulsed excitation is lifted because of the higher background in the pulse regime.

To study the performance of the SPEs in more details, we recorded a saturation curve from the emitter labeled SPE1 in Fig. 1B. More data are provided in the Supplementary Materials. Figure 2A shows the saturation behavior of SPE1 under cw laser excitation. The data are fit using the three-level system with an equation $I_{(P)} = I_\infty \times P/(P + P_s)$, where $I_{(P)}$ is the measured intensity count rate, P is the excitation power, and P_s (saturation power) and I_∞ (maximum count) are two fitting parameters. For this particular emitter, we obtain $P_s = 2.32 \pm 0.08$ mW and $I_\infty = 0.69 \pm 0.01 \times 10^6$ counts/s. Such a count rate is on par with the brightest RT SPEs from a bulk crystal. The detailed discussion of extraction efficiency analysis is given in Materials and Methods.

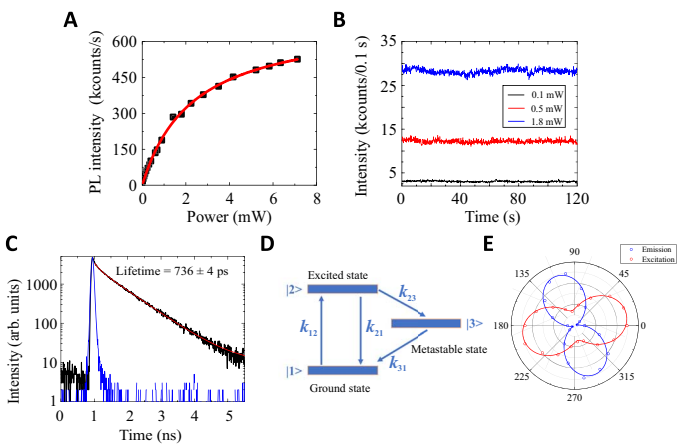


Fig. 2. Optical properties of SPE1. (A) Saturation curve of SPE1 yielding a saturation power $P_s = 2.32$ mW and $I_\infty = 0.69$ Mcounts/s. (B) Photon stability measurement at three different excitation powers of 0.1 mW (black curve), 0.8 mW (red curve), and 1.8 mW (blue curve), respectively, over a period of 2 min. The time resolution is 100 ms, and no obvious blinking has been observed. (C) Fluorescence lifetime measurement of SPE1 (black curve) fit with a single exponent (red curve) yielding a lifetime $\tau_1 = 736 \pm 4$ ps. The blue curve is the instrument response of the superconducting detector. (D) Schematic diagram of a three-level system used to describe the emitter. Detailed analysis of the transition rate can be found in the Supplementary Materials. (E) Polarization measurement of excitation (red open circle) and emission (blue open circle). The solid lines are the fitting with $\cos^2(\theta)$.

The source photostability is measured under low- and near-saturation excitation powers. The data are shown in Fig. 2B over an excitation period of 120 s under excitation powers of 0.1 mW (black curve), 0.5 mW (red curve), and 1.8 mW (blue curve). The time binning in this measurement is 100 ms, and no obvious blinking or bleaching was observed, proving the stability of the SPE. The fluorescence lifetime of the emitter is presented in Fig. 2C. The measured lifetime is 736 ± 4 ps (black curve), which is in accordance with the value obtained from the $g^{(2)}(\tau)$ fitting (776 ± 39 ps). The data were fit with single exponential function, and the instrument response function (blue curve) for our setup is shown for comparison in Fig. 2C. The system behaves according to a three-level model (Fig. 2D) with slight bunching at longer time scales (see the Supplementary Materials for the detailed rate equations). The polarization measurement of the emission and excitation is shown in Fig. 2E, fitting with $\cos^2(\theta)$. The polarization visibility $\eta = (I_{\max} - I_{\min})/(I_{\max} + I_{\min})$ of emission and excitation is calculated to be 93.2 and 55.4%, respectively, which shows that it is a single linearly polarized dipole transition. Note that the emission orientation does not necessarily align with the crystallographic axis of GaN. The histogram of the emission dipole orientation of additional emitters is shown in fig. S2. Likewise, the angle between the absorption and emission dipoles varies from emitter to emitter (fig. S2).

To further optimize the brightness of the SPE by means of improving the photon extraction efficiency, we take advantage of the rather mature fabrication techniques of GaN. Rather than using top-down reactive ion etching techniques, a separate GaN sample is grown on a patterned sapphire substrate (PSS). The scanning electron microscopy image of such a structure is shown in Fig. 3A. This structure is designed and extensively used for the light-emitting diode emission enhancement by increasing the reflection area and therefore improving the light extraction efficiency.